Current Trends in Biotechnology and Pharmacy
Vol. 20(2) 2913-2934 April 2026, ISSN 0973-8916 (Print), 2230-7303 (Online)
DOI: 10.5530/ctbp.2026.2.16

Homology modelling and structure-based screening of phenylacetamide derivatives targeting KLK-15 implicated in prostate cancer angiogenesis

Jyothi Bandi[1] and Navaneetha Nambigari[1,2]*

[1]Department of Chemistry, University College of Science, Osmania University, Saifabad, Hyderabad – 500 004 Telangana State, INDIA.
[2]Department of Chemistry, University College of Science, Osmania University, Tarnaka, Hyderabad – 500 007 Telangana State, INDIA.

***Corresponding author:** navaneeta@osmania.ac.in.

Abstract

Kallikrein like peptidase-15 (KLK-15) is a human tissue kallikrein protein, found to be expressed in prostate cancer through angiogenesis. KLK-15 acts on pro-uPA which initiates the activation of uPA, uPAR, by converting plasminogen into active plasmin, a proteolytic enzyme. The release of plasmin by KLK-15 is primarily accountable in support of Extracellular Matrix (ECM) degradation, and role of angiogenesis in cancer. Hence, using the KLK-15 protein as a novel target, we focussed on the study of its interaction with phenyl acetamide derivatives as anti-angiogenic agents. The current work involves the generation of 3D model of KLK-15 protein (256 amino acids) by using the homology modelling technique. The 3D model of the KLK-15 protein is MD Simulated and validated using Procheck, ProsA and Verify 3D server tools showing 91.04%, Z-Score = -6.03 and 80.86% parameters indicating the overall reliability of the generated model. Protein-Protein docking with its natural substrate (pro-uPA) identifies the active site residues. Virtual Screening using phenyl acetamide derivatives was performed by AutoDock 4.2 used through PyRx. The phenyl acetamide derivatives are likely to bind to the KLK-15 protein at His62, Tyr98, Arg101, His148, Glu206, and Ser209 amino acid residues. Based on the binding energy and physico-chemical data ligand L4:N-{5-[(3-methoxy benzyl)sulphanyl]-1,3,4- thiadiazol-2-yl}-2-2(4-methoxyphemnyl) acetamide, L7: N-{5-[(2-chlorobenzyl)sulfanyl]-1,3,4-thiadiazol-2-yl}-2-(4-methoxyphenyl) acetamide and ligand L10: N-{5-[(3-chlorobenzyl)sulfanyl]-1,3,4-thiadiazol-2-yl}-2-(4-methoxyphenyl) acetamide, may act as strong inhibitors against KLK-15 protein and act as a lead molecules against the pathological angiogenesis in prostate cancer.

Keywords-Kallikrein, Angiogenesis, Homology, Virtual screening.

Introduction

Worldwide cancer is found to be the principal reason of fatality (1,2). Cancer metastasis depend on angiogenesis, the sprouting of fresh blood vessels from existing surrounding blood vessels (3,4).This is regulated by activator molecules as a consequence of inputs received from the tumour cells and its surroundings. This is significant in view of the fact that the cancer growth relays on sufficient supply of oxygen and nutrients which is facilitated by the newly formed blood vessels (5). Kallikrein related Peptidases (KLKs) play a key role in various cancers by the formation of new blood vessels involving various pathways (6). KLKs induce angiogenesis by breaking proteins on ECM directly or through uPA/ uPAR signalling pathway indirectly (7). Thus targeting KLK signalling pathways can bring about the novel candidates to treat cancer.

Homology Modelling, virtual screening studies against novel anti angiogenic target of prostate cancer.

Current Trends in Biotechnology and Pharmacy
Vol. 20(2) 2913-2934 April 2026, ISSN 0973-8916 (Print), 2230-7303 (Online)
DOI: 10.5530/ctbp.2026.2.16

The tissue kallikreins (KLKs) contribute to the pathological angiogenesis. Plasma kallikrein is known to release kinins. (8) The Kallikrein gene and protein symbols are represented as *KLK* (written in Italics)and KLK (written in standard font) respectively (9). The tissue kallikreins can be classified into 15 proteases comprising of 244–282 amino acid residues and reported to have 40% identity among all KLKs. The first elucidated tissue kallikrein was represented as KLK-1; rest of them (KLK-2 to KLK-15) are called kallikrein-related proteases (10,11). The human KLKs are conserved serine peptidases and these proteins are pre - pro enzymes. The Pre sequence is having an amino-terminal signal, Pro means a pro-peptide an inactive zymogen and a serine-peptidase domain accountable for its biological activity (12).

In the present work KLK-15 protein which is found to be expressed in prostate cancer (13). KLK-15 is consistently reported to be up-regulated at the mRNA level in prostate cancer compared with benign tissue and worse progression-free survival (14). Multiple studies demonstrate that higher or aberrant KLK-15 expression is associated with biochemical relapse and progression after radical prostatectomy (15). These findings provide strong clinical evidence that KLK-15 deregulation is relevant in prostate tumor biology.

Thus KLK-15 is considered as novel target for the discovery of innovative lead molecules against angiogenesis. KLK-15 acts on pro-uPA, to convert inactive pro-uPA to active uPA (Urokinase-type Plasminogen Activator). The activation of uPA, and its receptor, uPAR (Urokinase-type Plasminogen Activator Receptor), which converts plasminogen into plasmin, an active proteolytic enzyme. This release of plasmin by KLK-15 is primarily accountable in support of ECM degradation through Matrix Metallo Proteinases (MMPs) pathway (16,17).

The biochemical pathway of KLK-15 is shown in Figure 1. *In-vitro* blocking of KLK-15 with specific small molecule inhibitors was found to inhibit the activation endothelial cell proliferation, migration, and development of branching cords. Hence, the current work focuses on the discovery of new small compounds as anti-angiogenic agents using the KLK-15 protein as a novel target.

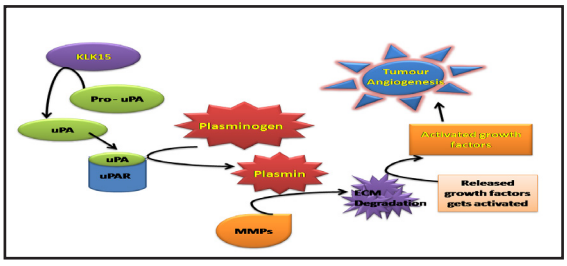

Figure 1: Biochemical pathway of KLK-15 protein: Activation of plasmin by KLK-15 via the uPA and uPAR activation, leading to the degradation of ECM components by MMPs to regulate tumour angiogenesis.

Materials and Methods

The current work focuses on the generation and evaluation of KLK-15 protein's 3D structure and virtual screening investigations to identify novel lead compound against the protein's active region.

Homology modelling is a technique for creating a 3D model of a protein by aligning template protein (experimentally known structure) coordinates with the target protein (no experimentally known structure) sequence (18). The initial step is to find a template protein that will be used to predict the structure of the protein of interest. The sequence alignment between the target protein and the template protein is the second step. The next stage is to create a 3D model, which is then optimised and validated. If required, the template identification, alignment, and model construction are performed repeatedly until an acceptable result is achieved (19).

ExPASy SwissProt (Expert Protein Analysis System) server (http://www.expasy.org) retrieves the KLK-15 protein amino acid sequence from the UniProtKB (Universal Protein Knowledgebase) database in FASTA format. UniProtKB provides information on protein sequence and function (20-24). In homology mod-

elling the first step is to choose a suitable template, which must be homologous to the target KLK-15 protein and have a crystal structure that exists in the Protein Data Bank (PDB) (25). Template search programmes like BLAST, JPred, HHpred are used to find templates based on the criteria of amino acid sequence identity, query coverage, and statistical E-value. The template is chosen by means of pairwise sequence alignment using Basic Local Alignment Search Tool (BLAST) (26-30). The BLAST server examines proteins fundamental biological sequence information for sequence similarities. JPred server uses the JNet algorithm to make predictions of coiled-coil region and residue solvent accessibility in the protein (31-34). It is used to measure the exactness of protein secondary structure prediction. The E-value is used to report the score values. HHpred is a server that predicts the sequence and secondary structure of proteins to implement pairwise comparison of profile Hidden Markov Models (HMMs) (35,36).

Once the template has been chosen, the KLK-15 protein sequence is aligned to the template protein sequence using the Clustal W 2.0 software (37,38).The resemblance among the KLK-15 protein and the template protein is identified by aligning them and verifying for the identical, similar and dissimilar residues. Clustal X program calculates identical and similar amino acid residues of the KLK-15 and template protein sequences. The alignment quality is measured by the percentage of identity and similarity. After sequence alignment between the target and template proteins, the KLK-15 protein 3D structure is built. The KLK-15 protein 3D structure is created using the MODELLER 9v9 programme (39,40). The protocol used to create the 3D model is by Satisfaction of Spatial Restraints (SSR) method (19). The model with lowest modeller objective function is chosen for further studies. The Swiss Protein Data Bank Viewer (SPDBV) is used to model the loop regions (41). To arrive at a stable structure, energy minimization is carried out to eliminate steric strains and collisions without causing major changes to the protein's overall structure (42,43).

Further the modelled protein quality is enhanced by locPREFMD server, which uses a method for local refinement of protein structures that focuses on improving local stereochemistry while conserving the overall fold. On the basis of the Cα root-mean-square deviation (Cα-RMSD), the structure with the lowest MolProbity score and the closest to the initial conformation is selected (44). locPREFMD focuses on local refinement, so restraints are essential. Post processing parameters are Physics-based energy (AMBER energy), Knowledge-based potentials and MolProbity validation. The server uses Force field: AMBER ff14SB, Water model: Implicit solvent GB and 5–10 independent 5 ns runs.

The validation of a 3D model is a decisive stage in determining the quality of a protein arrangement. The 3D model obtained after MD simulation is validated with various approaches for validation, such as the Ramachandran (RC) plot, which is an energy contour diagram from PROCHECK, the Verify 3D plot, and the Protein Structure Analysis (ProSA). The Psi (Ψ) and Phi (ϕ) angles for the 3D structure of the KLK-15 protein was calculated using PROCHECK server (45-47). Verify 3D assesses the stereo chemical quality of the KLK-15 protein structure using a scoring algorithm to determine the model's quality by graphing the sequence number against the 3D-1D score. The 3D models built which gave a Verify3D score value greater than 70% is a reliable quality model (48-50). The ProSA server is a validation tool for evaluating the overall model quality profile and the local model quality profile. The Z-score is a measure used by the ProSA server to assess the target protein's overall model quality. It compares protein stability to that of empirically determined (by NMR / X-ray crystallography) protein structures presently reported in the PDB (51). Further the target proteins are submitted to the PDBsum server for secondary structure analysis (52). The active sites and residues of proteins are predicted using Computed Atlas of Surface Topography of Proteins (CASTp) server (53,54). The CASTp server examines the functional

information of particular amino acid residues and active site areas of proteins by measuring pockets of 3D protein structures. The conserved domains of the target protein are also identified using NCBI-BLAST.

The protein protein docking study can reveal the nature of the binding site amino acid residues that are important in intermolecular interactions. Patch Dock server is a programme that predicts the structure of docked protein protein complex. In the present work 3D model of the KLK-15 is uploaded as the ligand input and the corresponding receptor input pro-uPA protein as receptor in the Patch Dock server (55-59).

Virtual screening (VS) is an important computational drug discovery method, which aids in the identification of novel drug candidates that are capable of binding to a target protein (60-63). The Virtual screening is carried out via AutoDock 4.2 used through PyRx (64). Docking settings are box center: 25 × 25 × 25 Å, Exhaustiveness – 8 and number of poses – 9 . Phenylacetamide derivatives with potential anti-cancer activity are chosen as small *in-house* database (65). The phenylacetamide structures are found in the Pub Chem database (66). The *in-house* library of ligand molecules are optimized with MMFF94 and CHEMICAL force fields of the Open Babel software for screening. The phenylacetamide ligands were converted to SDF file format. The Conjugate Gradient and Steepest Descent optimization algorithms (50000 steps with the 0.001 kcal/mol/Angstrom convergence criterion) are used for energy minimization. Finally, the option 'all ligand' was used to convert the minimized files to .pdbqt format to produce their atomic coordinates for docking. The results from screening runs are the best predicted binding modes and corresponding binding affinity. The more negative numerical values for the binding affinity (top 10), the better is the predicted binding between a ligand and the target protein (67).

Molecules with unfavourable ADME have been identified as a primary cause of failure of drug candidate molecules in drug development procedures (68-70). ADME predictions avoid drug molecule failures in the drug development stage (71). Predicted ADME properties include molecular weight, donor hydrogen bond descriptor values, number of acceptor hydrogen bonds, percentage of human oral absorption (72,73), Lipinski's rule of five (LROF) (74), and Lipinski's rule of three (LROT) (75) are considered for further evaluation of the ligand molecules. The top ten molecules of the virtual screening with an acceptable binding energy were further evaluated for pharmacokinetic properties using Swiss ADME server (76). The new Swiss ADME web tool, allows to compute physico-chemical descriptors as well as to predict ADME parameters, physico-chemical properties, pharmacokinetics, drug-likeness, and medicinal chemistry friendliness, including in-house expert methods like the BOILED-Egg (77), iLOGP (78), and Bioavailability Radar to support drug discovery.

Results and Discussions:

This section focuses on the 3D model analysis and validation as per our protocols (79,80). The fasta sequence of the KLK-15 protein, which has the Uniprot ID Q9H2R5 sequence (256 amino acids), was downloaded from the ExPASy server and is uploaded for template protein search on servers as shown in Table1.

Table 1: KLK-15 protein – Template selection.

S. No.	Server	Parameter(s)	E-Value	PDB CODE
1	BLAST	Sequence Specificity	7e – 79	1NPM – A
2	Jpred 4	Secondary Structure	1e – 64	1NPM - A
3	HH - Pred	Sequence, Secondary Structure	4.6e – 31	1NPM - A

1NPM-A is selected as template protein based on sequence & structure similarity, as reflected in E-value

The results received from NCBI-BLASTp, Jpred4, and HHPred data analysis, has a lowest E-value of 7e-79, 1e-64 and 4.6e-31 for a common template, the Neuropsin PDB ID: 1NPM-A was utilised as the template protein for modelling the KLK-15 protein. 1NPM-A has query coverage of 90% and 49.36% of identity with the KLK-15 protein sequence. Based on sequence comparison, secondary structure and fold recognition characteristics a template protein can be selected that is comparable to the KLK-15 protein sequence. The template protein is assessed using the percentage identity, query coverage and E-value as criterion. 1NPM-A was verified as a legitimate template based on the findings acquired from the template search data analysis. 1NPM-A was downloaded from the RCSB PDB for generating the 3D structure of the target protein.

Figure 2 illustrates that the KLK-15 protein sequence was aligned with the template 1NPM-A protein sequences using the Clustal W 2.0 software. The resemblance identified by aligning target and template sequences is found to have 112 conserved amino acid residues 43.75%. 47amino acids (18.35%) are strongly similar, 27 amino acids (10.54%) are weakly similar and diverse amino acids constitute for 27.34%.

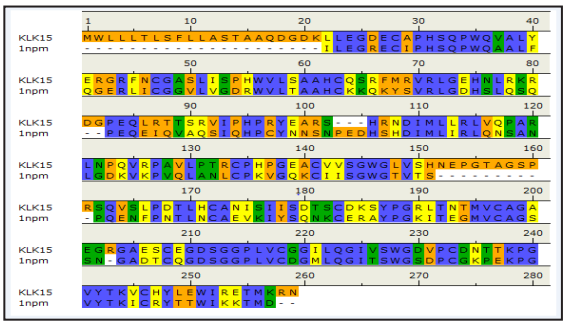

Figure 2: KLK-15 protein and the template 1NPM-A pair wise alignment: *Pair wise sequence alignment of* KLK-15 *sequence with its templates was carried out with CLUSTAL W and visualized in Discovery Studios 3.5.The figure depicts conserved amino acid residues indicated with blue color, strongly similar with yellow color, Weakly Similar with green color and orange color for Diversity.*

The quality of alignment is measured by the percentage similarity of the alignment between KLK-15 and 1NPM-A, was found to be 72.64%. With the help of Modeller 9v9 program the initial 3D model of KLK-15 protein was constructed. Out of two hundred (200) models that are developed, the model with the smallest possible modeller objective function (1763.7673) was chosen for further validation.

Table 2. Molecular dynamics parameters of the 3D Model of KLK-15.

S. No.	Parameter Checked	Initial Value	Refined Value	Goal
1	Phi -psi backbone favoured region	83.500	91.04	> 90 %
2	Phi-psi backbone allowed region	16.000	8.02	-
3	Phi-psi backbone general region	1.500	0.94	< 1 %
4	Phi-psi backbone unfavoured region	0.035	0.000	< 0.2 %
5	chi1-chi2 side chain disallowed region	0.007	0.021	< 0.2 %
6	G-factor covalent bonds	0.180	0.130	> -0.5
7	G-factor overall interactions	-0.110	-0.200	> -0.5
8	Favourable main chain bond lengths	100.000	100.000	100 %
9	Favourable main chain angles	96.300	93.700	100 %
10	Side chain ring planarity	72.00	96.600	100 %

The structure of the KLK-15 *protein after energy minimization is further stabilized by carrying out a molecular dynamics study in locPREFMED server tool. The values obtained show that the dynamically stabilized structure of* KLK-15 *has the most stable conformation.*

Homology Modelling, virtual screening studies against novel anti angiogenic target of prostate cancer.

Current Trends in Biotechnology and Pharmacy
Vol. 20(2) 2913-2934 April 2026, ISSN 0973-8916 (Print), 2230-7303 (Online)
DOI: 10.5530/ctbp.2026.2.16

The 3D model of KLK-15 is improved via loop modelling utilising SPDBV4.1.0, using a conjugate gradient technique by which the poor contacts are computed. Energy minimization is carried out by adding hydrogens to the 3D model. The final 3D model was analysed and carried out by using loop build module and energy minimization using Swiss PDB Viewer 4.1.0. The minimum of energy for the modified KLK-15 model is -14271.58 KJ/mol.

The model's superiority is further enhanced by using the locPREFMD online server to perform molecular dynamic simulations. Table 2 displays the KLK-15 Molecular dynamics refinement data collected from the locPREFMD server, the total refined factors after the simulations. The molprobity score refined from 1.742 to 1.262 after refining using MD simulation.

The KLK-15 protein structure stereo chemical quality was confirmed using the RC plot obtained, which mentions the Psi (Ψ) and Phi (ϕ) angles from PROCHECK server. The favoured region is depicted in red, while furthermore permissible region is depicted in brown, the generously permitted zone is depicted in yellow, and the banned zone is depicted in white.

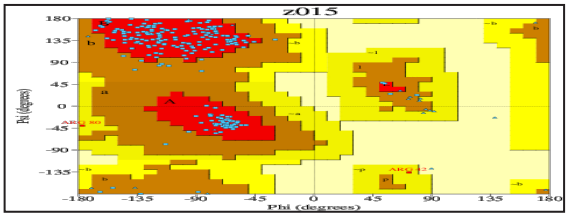

Figure 3: Ramachandran Plot of the KLK-15 protein.

The RC plot of the KLK-15 protein's is shown in Figure 3 depicts that 91.04 percent of residues are in the most preferred red region, 8.02 percent in the additionally allowed brown region, 0.94 percent in the generously allowed yellow region, and none in the disallowed white region. This confirms that the three dimensional structure of KLK-15 protein is a valid model.

The ProSA tool is used to estimate the overall fold and model quality. The secondary structural characteristics and probable active site regions of the KLK-15 protein's most stable conformation are reported. The overall and local model quality of the KLK-15 protein, as illustrated in Figure 4, is verified by comparing it to the structures of proteins with similar amino acid lengths that have been published in the PDB. The total folding energies of KLK-15 protein are strongly negative, with a Z-score of -6.03, which is shown as a black point within the Dark blue area, implies that the KLK-15 model is particularly similar to the experimentally obtained NMR structures.

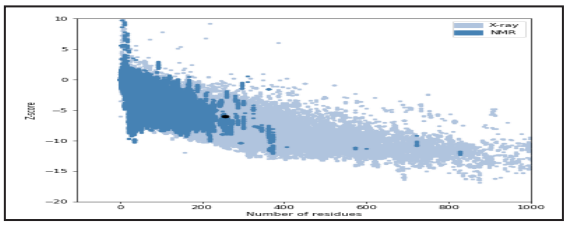

Figure 4: Stereo chemical quality of the KLK-15 protein:*Overall and local model quality assessment of the* KLK-15*. The Z-score (Black dot) obtained from ProSA server for the* KLK-15 *protein is -6.03. The ProSA plot represented for all the proteins in PDB determined by X-ray crystallography (light blue) and by NMR Spectroscopy (dark blue).*

The protein energy is shown in two portions in Figure 5, with window sizes of 10 to 40 amino acids. The small energy profile that identifies KLK-15 protein's local model quality is acceptable. As a result, the created 3D model of KLK-15 is chemically and energetically stable.

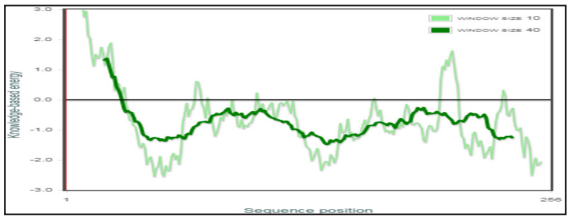

Figure 5: Energy profile of KLK-15 protein. The knowledge-based energy profile of the individual amino acids on a window size 10 amino acids (light green) and window size 40 amino acids (dark green).

Current Trends in Biotechnology and Pharmacy
Vol. 20(2) 2913-2934 April 2026, ISSN 0973-8916 (Print), 2230-7303 (Online)
DOI: 10.5530/ctbp.2026.2.16

Verify 3D analyses the stereo chemical quality of the KLK-15 protein structure using a scoring algorithm. 80.86% of the amino acids have average 3D-1D score ≥ 0.2 is shown in Figure 6. This again confirms that the stereo chemical structure of KLK-15 protein is a reliable model.

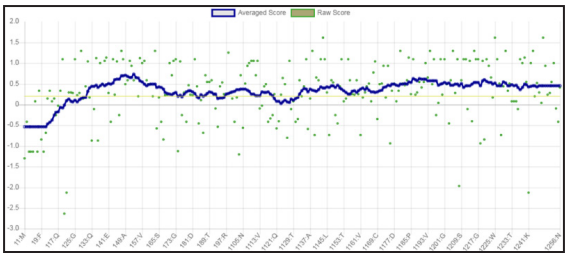

Figure 6: Verify 3D of KLK-15 Protein. *The plot shows 80.86% of the residues have 3D-1D score ≥ 0.2.*

KLK-15 protein is submitted to the PDB sum server for secondary structure analysis. It has three (3) helices, fifteen (15) beta sheets, six (6) disulphide bonds and eight (8) beta hairpins, as shown in Figure 7 and Table S1 (Supplementary Information).

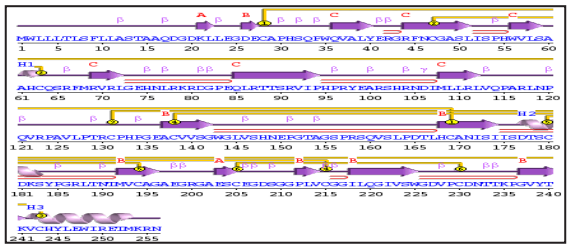

Figure 7: Secondary structure elements of KLK-15 protein: The secondary structure as obtained in PDB Sum for KLK-15. The KLK-15 protein secondary structure shows 3 α helices, 15 β sheets, 6 disulphide bonds and 8 β hairpins.

The secondary stucture of KLK - 15 shows the presence of alpha helix (Ala61-Cys63) and second helix from Asp177-Ser183 and Val242-Met253. And also 15 beta sheets comprising of Lys21-Leu23, Asp26-Glu27, Gln36-Glu41, Arg44-Leu51, Trp56-Ser59, Arg69-Leu72, Gln85-Pro94, Met108-Leu112, Ala137-Gly142, His168-Ile174, Met192-Gly196, Glu203-Cys205, Pro212-Cys215, Ile218-Trp225 and Gly237-Lys241.

Furthermore, secondary structure of the KLK-15 protein model revealed the presence of five salt bridges Lys79-Asp81 (3.236 and 3.601 Å), Arg71-Glu84 (3.374 and 3.104 Å) and Asn227-Lys235 (3.459 Å); two pi-pi Trp225-His103 (3.67 and 3.82 Å); one pi-sigma Trp56-Met253 (3.73 Å); and six weak pi-cation Tyr184-Lys235 (5.06 Å), Tyr40-Arg71 (3.89 and 5.76 Å), Trp2-Met1 (5.41 and 5.01Å) and His148-Lys21 (4.40 Å) interactions shown in Table 3. According to the secondary structure analysis, the resulting model is a structurally stable and reliable model.

Table. 3 Intramolecular Interactions in KLK-15 protein.

S. No.	Interaction Type	Residues involved	Distance in Å
1	Pi-Pi	Trp225 – His103	3.67
2	Pi-Pi	Trp225 – His103	3.82
3	Pi- cation	Tyr184 – Lys235:NZ	5.06
4	Pi- cation	Tyr40 – Arg71:NH1	3.89
5	Pi- cation	Tyr40 – Arg71:NH2	5.76
6	Pi- cation	Trp2 – Met1:N	5.41
7	Pi- cation	Trp2 – Met1:N	5.01
8	Pi- cation	His148 – Lys21:NZ	4.40
9	Pi- sigma	Trp56 – Met253:CG	3.73
10	Salt Bridge	Lys79 – Asp81	3.236
11	Salt Bridge	Lys79 – Asp81	3.601
12	Salt Bridge	Arg71 – Glu84	3.374
13	Salt Bridge	Arg71 – Glu84	3.104
14	Salt Bridge	Asn227 – Lys235	3.459

The kallikrein family of proteins, KLK-1, has the same secondary structure of 15 beta sheets and 8 beta hairpins; KLK-2, has the same secondary structure of 3 helices and 8 beta hairpins; KLK-7, KLK-8, and KLK-10 has the same secondary structure of 8 beta hairpins and 6 disulphide linkages. The 3D structure of the protein KLK-15 is depicted in Figure8.

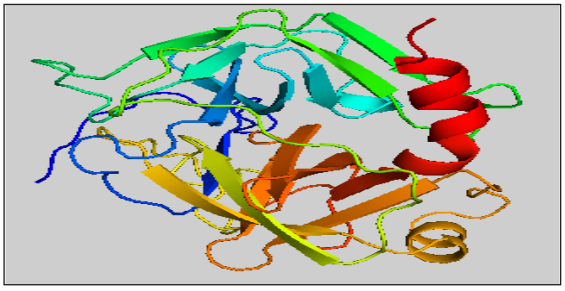

Figure 8: The 3D Model of KLK-15 Protein showing secondary structure of 15 strands and 3 helices.

The recognition of the biologically active area is a crucial phase in the medicine development process. In order to analyse the active site domain, this server examines the size and capacity of each pocket. The KLK-15 protein sequence contains a Trypsin like serine protease (Tryp_SPc) conserved domain as per the findings found from NCBI – BLASTp server. The conserved domain amino acids range from Gly25 to Arg250 is revealed in Figure 9.

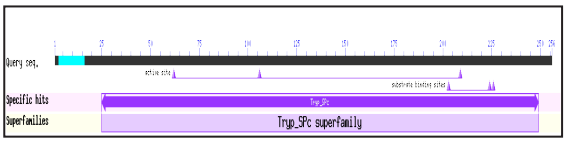

Figure 9: Conserved domain of the KLK-15 protein: The pictorial representation of local similarity search result obtained by BLAST shows that the putative the presence of Trypsin like serine protease (Tryp_SPc) domain, which is involved in activation of pro-uPA by KLK-15 protein.

The CASTp server is used to visualize the active site domains of the KLK-15 protein significant in the signalling cascade. The CASTp server data indicates the presence of two binding pockets and residues are given in Table 4. The big hydrophobic section covers 29 amino acids with a volume of 764.01 Å^3 and the small pocket covers 8 amino acids with a volume of 57.479 Å^3 at the active site domain area of the KLK-15 protein. CASTp server data suggest that the N-terminal region is the active site pocket of the KLK-15 protein.

Table 4. Amino acid residues in the binding pockets of KLK-15 protein.

Pocket No.	**CASTp**		
	Volume(Å^3)	Amino acid residues	No. of Amino Acids in the pocket
1	764.018	Glu206, Leu163, Ser162, Val161, Glu160, Arg158, Pro151, Asn19, His148, Leu145, Arg44, Lys21, Asp20, Gly19, Asp18, Glu17, Ala16, Ala15, Thr14, Ser13, Leu11, Leu10, Phe9, Leu7, Leu5, Leu, Leu3, Trp2, Met1	29
2	57.479	Ser53, Pro54, His55, Trp56, Arg250, Met253, Lys254, Arg255	8

Amino acid residues in the binding pockets of KLK-15 *protein as obtained from CASTp Server with its volume.*

The Patch Dock server programme with the Fast Fourier Transformation approach is used to perform protein – protein docking. The docking inputs are the 3D model of KLK-15 protein and pro-uPA receptor protein (PDBID: 1C5W). Before adding polar hydrogen atoms, all hetero atoms, including water, were removed from the receptor pro-uPA. The PDB files for receptor and KLK-15 were submitted in patch dock. The RMSD was set to 4 Å and remaining settings were as default. To confirm the binding interactions predicted the docked complex of KLK-15 and pro-uPA is investigated to reveal the active amino acid residues responsible in the binding.

Table 5. Intermolecular interactions of KLK-15 and pro- uPA.

S. No	Bond	Amino acid residues KLK-15 and pro-uPA	Distance (Å)
1	Hydro-gen Bond	Gly226:O – B:Arg36:HH21	2.4941
		Glu206:OE1 – B:Arg37A:N	2.0306
		Glu206:OE2 – B:Arg37A:N	1.7044
		Glu206:OE1 - B:Gly37B:N	2.37053
		Glu206:OE2 - B:Gly37B:N	2.0425
		Ala100:O - B:Lys61:HZ2	2.1469
		Val228:O - B:Lys82:HZ1	1.8601
		Val228:O - B:Lys82:HZ2	2.1659
		Arg101:HH11 - B:Pro60C:O	2.3513
		Arg101:HH12 - B:Pro60C:O	2.4671
		Gly152:H - B:Asn74:O	1.9096
		Ala154:H - B:Asn76:OD1	2.18
		Arg187:HH11 - B:Glu84:OE1	2.0338
		Arg187:HH11 - B:Glu84:OE2	1.2244
		Arg187:HH12 - B:Glu84:OE1	2.3990
		Arg187:HH12 - B:Glu84:OE2	2.1359
2	Pi-Cation	His62 - B:Arg37A:NH1	5.6496
		His62 - B:Arg37A:NH2	4.3062

There are two pi-cation, His62-Arg37 (distance of 4.3062 and 5.696 Å) and sixteen strong hydrog

en bond interactions in the distance range from 1.2244 to 2.4941 Å in the docked complex of KLK-15 – pro-uPA proteins, shown in Table 5. The interacting amino acids are His62, Ala100, Arg101, Gly152, Ala154, Arg187, Glu206, Gly226, and Val228 which fall in the conserved domain area of KLK-15 protein, have been identified as crucial for binding.

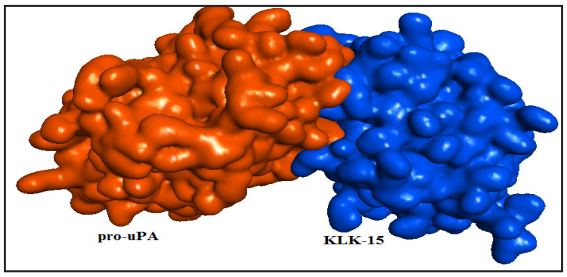

Figure 10: Docked complex of KLK-15 and pro-uPA in surface mode: Surface mode representation of docked complex of KLK-15 and pro-uPA. KLK-15 is in blue color and pro-uPA in brown color.

Figure 10, depict the surface interaction mode.It is assumed that the area of KLK-15 from Arg101 to Gly226 and His62 (one of the catalytic triad residues) works as an active site residues responsible for angiogenesis signalling based on the findings of the Protein – protein investigation (PPI).

The 3D structure of the KLK-15 protein is subjected to virtual screening to identify new lead compounds Virtual screening is performed by AutoDock 4.2 used through PyRx software. KLK-15 protein 3D structure has been submitted in PDB format and automatically the structure is cleaned and pre-processed. The protein preparation, ligand database preparation, and docking procedures are all part of the Virtual screening technique. KLK-15's 3D structure has been uploaded in PDB format. The autodock tools will convert the uploaded 3D protein file from .pdb to .pdbqt format. Phenylacetamide derivatives are chosen as *in-house* database are obtained from the Pub Chem database. The various force fields of the Open Babel programme are used to optimise the *in-house* library of ligand molecules. Energy minimization is achieved using

the Conjugate Gradient and Steepest Descent optimization methods.

The KLK-15 protein's conserved domain region (Grid Box : 25 × 25 × 25 Å) was virtually screened, generating phenylacetamide ligand molecules in nine different poses. To score the docking poses and rank the ligands, the Vina empirical scoring function is employed. In order to choose the top candidates based on binding energies and physico-chemical characteristics, the nine highest-scoring postures from the top 10 phenylacetamide compounds were chosen and visualized using Accelrys Discovery Studio Visualizer 3.5.

According to the results of virtual screening, Phenylacetamide derivatives show a significant affinity for the KLK-15 protein, with binding energy in the range from -7.6 to -6.2 kcal/mol (79-81). Figure S1, depicts the interactions of the top ten ligand molecules (L1 to L10) like intermolecular interactions. Hydrogen bond and Pi interactions exist between the new scaffolds molecules are in the conserved domain region of KLK-15 as well as the amino acids His62 and Ser209 of catalytic triad and also the other residues such as Tyr98, Arg101, His148, and Glu206 of the active pocket.

Table 6 shows the intermolecular interactions between the lead ligands and the active amino acid residues with its bond length. Table S2, shows the structure of ligand molecules together with their energy values and RMSD.

The ligands L5, L6 & L9 are simple acetamide derivatives whereas the ligands L1, L2, L3, L4, L7, L8 & L10 are thiadiazole acetamide derivatives. The residues His62, Tyr98, Arg101, His148, Glu206 and Ser209 have interactions with the ligand molecules, indicating that they are biologically active in the KLK-15 protein. His62 and Ser209 are the catalytic residues in KLK-15 which have interactions with many of these ligands (L1 to L10). The results reveal that there are hydrogen bond interactions (ranging 1.9110 to 2.4914 Å), Pi-Pi (ranging 3.8112 to 4.2043 Å), Pi-Sigma (at a distance of 3.7105 Å), and Pi-Cation (ranging 4.9814 to 6.6631 Å) interactions.

Table 6. Ligand interactions with KLK-15.

S. No.	Ligand	Interacting Residue	Bond Length (Å)	Interaction Type
1	L1	Glu206:OE2	2.4082	Hydrogen Bond
2	L2	Tyr98:OH	2.0329	Hydrogen Bond
		Tyr98:HH	2.3843	Hydrogen Bond
		His62	4.9814	Pi-Cation
3	L3	Tyr98:OH	2.1638	Hydrogen Bond
		Tyr98:HH	1.9110	Hydrogen Bond
		Tyr98:HH	2.2037	Hydrogen Bond
		Ser209:HG	2.2368	Hydrogen Bond
4	L4	Ser209:HG	2.1799	Hydrogen Bond
5	L5	His62:NE2	1.9887	Hydrogen Bond
		Ser209:HG	2.0475	Hydrogen Bond
		His62	4.0742	Pi-Pi

6	L6	His62	4.2043	Pi-Pi
7	L7	Tyr98:OH	2.4251	Hydrogen Bond
		Tyr98:HH	2.1976	Hydrogen Bond
		Tyr98:HH	2.0961	Hydrogen Bond
		His62	3.7105	Pi-Sigma
8	L8	Tyr98:OH	2.1948	Hydrogen Bond
		Tyr98:HH	2.0768	Hydrogen Bond
		Tyr98:HH	2.0480	Hydrogen Bond
		His62	3.8112	Pi-Pi
9	L9	His62	4.1622	Pi-Pi
10	L10	Ser209:HG	2.4914	Hydrogen Bond
		His62	3.9577	Pi-Pi

The ligand molecules are prioritized based on binding energies, RMSD, ligand interactions with a visual inspection. All the have interaction which indicates, they can bind and inhibit KLK-15 protein and act as antagonists for pathological angiogenesis.

ADME Analysis

Prior to preclinical testing, ADME screening is an essential step in the medicine development method. The ADME of the ligand is evaluated for their physico-chemical properties via SWISS ADME server indicte they obey lipinski's rule of five and jorgensen's rule of three indicates that they are highly absorbed and bio available. Table 7 show indicate the permissible values of physico-chemical parameters, a positive logP value indicative of the lipophilicity and permissible TPSA.

Table 7. Predicted ADME properties of the docked molecules

Ligand No.	Is Lead Like	HBA	HBD	Logp	MW	TPSA
L1	Y	8	1	2.24	454.45	154.24
L2	Y	6	1	2.38	416.47	163.47
L3	Y	7	1	2.89	439.47	117.65
L4	Y	5	1	2.68	401.5	126.88
L5	Y	3	1	2.48	259.28	38.33
L6	Y	3	1	2.37	247.24	29.1
L7	Y	4	1	2.87	405.92	117.65
L8	Y	5	1	2.98	401.5	126.88
L9	Y	2	1	2.56	263.69	29.1
L10	Y	4	1	2.96	405.92	117.65

The permissible ADME values are as follows: MW< 500, HBD< 5, HBA<10, logp < 5.6, TPSA ≤ 120Å.

Current Trends in Biotechnology and Pharmacy
Vol. 20(2) 2913-2934 April 2026, ISSN 0973-8916 (Print), 2230-7303 (Online)
DOI: 10.5530/ctbp.2026.2.16

The ligands L3, L5, L6, L7, L9 and L10 although have permissible TPSA value are suitable for Non-CNS category of drugs. Ligands L1, L2, L4 and L8 have non-permissible TPSA (>120 Å) indicating that these can easily cross the blood-brain barrier. Figure 11 illustrates the Bioavailability Radar plots for the L1–L10 displaying rapid appraisal of drug-likeness. Bioavailability plot takes into account six physicochemical properties: Lipophilicity,size, polarity, solubility, flexibility and saturation. A physicochemical range on each axis was defined by descriptors adapted and depicted as a pink area in which the radar plot of the molecule has to fall entirely to be considered druglike (81,82).

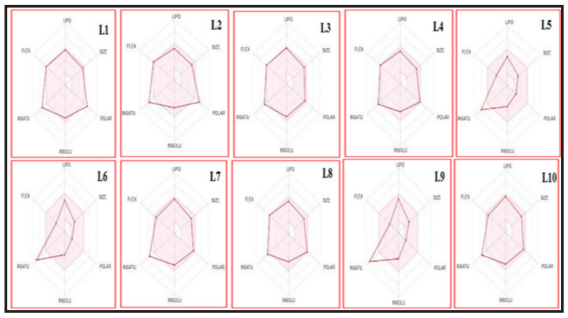

Figure 11: Bioavailability Radar plot

The BOILED Egg prediction plot which is based on TPSA vs. log p, shown in Figure S2 (Supplementary Information). The yellow zone (yolk) is the physico-chemical space with the greatest possibility of molecules penetrating to the brain, whereas the white region is the physico-chemical space with the greatest likelihood of chemicals being absorbed by the gastrointestinal system. Therefore, ligands L4, L7 and L10 found to be hydrophilic and suitable as oral inhibitors. Since the ligands L5, L6, L8 and L9 were found to cross the BBB and L1, L2 and L3 were found to be outside the bioavailability zones, indicating that are not suited for non-CNS category medicines. All ten ligands are found to be the substrates of phosphor glycol protein. Substrates of P-glycoprotein (PGA) are susceptible to changes in pharmacokinetics due to drug interactions with P-gp inhibitors or inducers.PGA overexpression is one of the main mechanisms behind decreased intracellular drug accumulation in various cancers, in this case it is P-gp -.The pink area represents the optimal range for each properties (Lipophilicity: XLOGP3 between − 0.7 and + 5.0, size: MW between 150 and 500 g/mol, polarity: TPSA between 20 and 130 *Å*, solubility: log S not higher than 6, saturation: fraction of carbons in the sp3 hybridization not less than 0.25, and flexibility: no more than 9 rotatable bonds. L1, L2, L4, L5, L6, L8 andL9 are predicted to be not orally bioavailable, because too flexible and too polar.

Based on the results of virtual screening, ADME data the ligands L4, L7 and L10 are found to be more drug-like properties, synthetic feasibility and can be exploited to generate new inhibitors for the KLK-15 protein.

Conclusions

The 3D structure of the KLK-15 protein built using 1NPM-A as a template and further refined using LocPREFMD server for a high quality structure. Further validation is confirmed using Procheck, ProsA and Verify 3D server tools showing 91.04%, Z-Score = -6.03 and 80.86% parameters indicating the overall reliability of the generated model. The binding residues His62, Tyr98, Arg101, His148, Glu206 and Ser209 in the biological active site domain of the KLK-15 protein are identified by the protein – protein interaction studies of KLK-15 with uPA.

The binding energy and physio-chemical features of the novel lead compounds (L1 to L10) are selected. The novel ligand compounds with an acceptable range of pharmacokinetic characteristics found by virtual screening have functional groups methoxy phenyl and thiadiazole as the common pharmacophore moieties. L4:N-{5-[(3-methoxy benzyl)sulphanyl]-1,3,4- thiadiazol-2-yl}-2-2(4-methoxyphemnyl) acetamide, L7: N-{5-[(2-chlorobenzyl)sulfanyl]-1,3,4-thiadiazol-2-yl}-2-(4-methoxyphenyl) acetamide and ligand L10: N-{5-[(3-chlorobenzyl)sulfanyl]-1,3,4-thiadiazol-2-yl}-2-(4-methoxyphenyl)acetamide molecules with accept-

able ADME values, may function as potent inhibitor for KLK-15 protein and act as lead candidates for future designing against the pathological angiogenesis in prostate cancer.

Acknowledgements

The Authors, JB and NN are thankful to the Head, Department of Chemistry and Principal, University College of Science, Saifabad, Osmania University, Hyderabad, Telangana for providing Research Facilities. The Authors are thankful to the DST FIST, New Delhi, INDIA for facility of the Computational Lab at Department of Chemistry, University College of Science, Saifabad, Osmania University, Hyderabad, Telangana, INDIA.

Author contributions

JB: “Data curation, Formal analysis, Investigation; Validation; Visualization”; NN: Data Interpretation and Roles/Writing–review & editing.

Conflict of interest

The corresponding author states that there is no conflict of interest.

Funding

No financial support from any agency.

Availability of data and material/data availability

All data generated or analysed during this study are included in this published article [and its supplementary information files].

References

1. Carmeliet, P. (2005). Angiogenesis in life, disease and medicine. *Nature*, *438*(7070), 932-936.
2. American Cancer Society. (2022). Cancer Facts & Figures 2022. Atlanta: American Cancer Society
3. Hanahan, D., & Weinberg, R. A. (2011). Hallmarks of cancer: the next generation. *Cell*, *144*(5), 646–674. https://doi.org/10.1016/j.cell.2011.02.013
4. Liotta, L. A., & Kohn, E. C. (2001). The microenvironment of the tumour-host interface. *Nature*, *411*(6835), 375–379. https://doi.org/10.1038/35077241
5. Nishida, N., Yano, H., Nishida, T., Kamura, T., & Kojiro, M. (2006). Angiogenesis in cancer. *Vascular health and risk management*, *2*(3), 213–219. https://doi.org/10.2147/vhrm.2006.2.3.213
6. Emami, N., & Diamandis, E. P. (2007). Human tissue kallikreins: a road under construction. *Clinica chimica acta; international journal of clinical chemistry*, *381*(1), 78–84. https://doi.org/10.1016/j.cca.2007.02.023
7. Yousef, G. M., & Diamandis, E. P. (2002). Human tissue kallikreins: a new enzymatic cascade pathway?. *Biological chemistry*, *383*(7-8), 1045–1057. https://doi.org/10.1515/BC.2002.113
8. Kalinska, M., Meyer-Hoffert, U., Kantyka, T., & Potempa, J. (2016). Kallikreins - The melting pot of activity and function. *Biochimie*, *122*, 270–282. https://doi.org/10.1016/j.biochi.2015.09.023
9. Diamandis, E. P., Yousef, G. M., Clements, J., Ashworth, L. K., Yoshida, S., Egelrud, T., Nelson, P. S., Shiosaka, S., Little, S., Lilja, H., Stenman, U. H., Rittenhouse, H. G., & Wain, H. (2000). New nomenclature for the human tissue kallikrein gene family. *Clinical chemistry*, *46*(11), 1855–1858
10. Koumandou, V. L., & Scorilas, A. (2013). Evolution of the plasma and tissue kallikreins, and their alternative splicing isoforms. *PloS one*, *8*(7), e68074. https://doi.org/10.1371/journal.pone.0068074
11. Lilja H. (1985). A kallikrein-like serine protease in prostatic fluid cleaves the predominant seminal vesicle protein. *The Journal of clinical investigation*, *76*(5), 1899–1903. https://doi.org/10.1172/JCI112185
12. Webber, M. M., Waghray, A., & Bello, D. (1995). Prostate-specific antigen, a serine protease, facilitates human prostate cancer cell invasion. *Clinical cancer research : an official journal of the American Asso-*

ciation for Cancer Research, *1*(10), 1089–1094.

13. Yousef, G. M., Scorilas, A., Jung, K., Ashworth, L. K., & Diamandis, E. P. (2001). Molecular cloning of the human kallikrein 15 gene (KLK15). Up-regulation in prostate cancer. *The Journal of biological chemistry*, *276*(1), 53–61. https://doi.org/10.1074/jbc.M005432200
14. Yousef GM, Scorilas A, Jung K, Ashworth LK, Diamandis EP. Molecular cloning of the human kallikrein 15 gene (KLK15). Up-regulation in prostate cancer. J Biol Chem. 2001 Jan 5;276(1):53-61. doi: 10.1074/jbc.M005432200. PMID: 11010966.
15. 17. Rabien A, Fritzsche FR, Jung M, Tölle A, Diamandis EP, Miller K, Jung K, Kristiansen G, Stephan C. KLK15 is a prognostic marker for progression-free survival in patients with radical prostatectomy. Int J Cancer. 2010 Nov 15;127(10):2386-94. doi: 10.1002/ijc.25435. PMID: 20473923.
16. Takayama, T. K., Carter, C. A., & Deng, T. (2001). Activation of prostate-specific antigen precursor (pro-PSA) by prostin, a novel human prostatic serine protease identified by degenerate PCR. *Biochemistry*, *40*(6), 1679–1687. https://doi.org/10.1021/bi002129r
17. Borgoño, C. A., & Diamandis, E. P. (2004). The emerging roles of human tissue kallikreins in cancer. *Nature reviews. Cancer*, *4*(11), 876–890. https://doi.org/10.1038/nrc1474
18. Cavasotto, C. N., & Phatak, S. S. (2009). Homology modeling in drug discovery: current trends and applications. *Drug discovery today*, *14*(13-14), 676–683. https://doi.org/10.1016/j.drudis.2009.04.006
19. Sali, A., & Blundell, T. L. (1993). Comparative protein modelling by satisfaction of spatial restraints. *Journal of molecular biology*, *234*(3), 779–815. https://doi.org/10.1006/jmbi.1993.1626
20. UniProt Consortium (2015). UniProt: a hub for protein information. *Nucleic acids research*, *43*(Database issue), D204–D212. https://doi.org/10.1093/nar/gku989
21. Artimo, P., Jonnalagedda, M., Arnold, K., Baratin, D., Csardi, G., de Castro, E., Duvaud, S., Flegel, V., Fortier, A., Gasteiger, E., Grosdidier, A., Hernandez, C., Ioannidis, V., Kuznetsov, D., Liechti, R., Moretti, S., Mostaguir, K., Redaschi, N., Rossier, G., Xenarios, I., … Stockinger, H. (2012). ExPASy: SIB bioinformatics resource portal. *Nucleic acids research*, *40*(Web Server issue), W597–W603. https://doi.org/10.1093/nar/gks400
22. Gasteiger, E., Gattiker, A., Hoogland, C., Ivanyi, I., Appel, R. D., & Bairoch, A. (2003). ExPASy: The proteomics server for in-depth protein knowledge and analysis. *Nucleic acids research*, *31*(13), 3784–3788. https://doi.org/10.1093/nar/gkg563
23. Boeckmann, B., Bairoch, A., Apweiler, R., Blatter, M. C., Estreicher, A., Gasteiger, E., Martin, M. J., Michoud, K., O'Donovan, C., Phan, I., Pilbout, S., & Schneider, M. (2003). The SWISS-PROT protein knowledgebase and its supplement TrEMBL in 2003. *Nucleic acids research*, *31*(1), 365–370. https://doi.org/10.1093/nar/gkg095
24. Boutet, E., Lieberherr, D., Tognolli, M., Schneider, M., Bansal, P., Bridge, A. J., Poux, S., Bougueleret, L., & Xenarios, I. (2016). UniProtKB/Swiss-Prot, the Manually Annotated Section of the UniProt KnowledgeBase: How to Use the Entry View. *Methods in molecular biology (Clifton, N.J.)*, *1374*, 23–54. https://doi.org/10.1007/978-1-4939-3167-5_2
25. Berman, H. M., Battistuz, T., Bhat, T. N., Bluhm, W. F., Bourne, P. E., Burkhardt, K., Feng, Z., Gilliland, G. L., Iype, L., Jain, S., Fagan, P., Marvin, J., Padilla, D., Ravichandran, V., Schneider, B.,

Thanki, N., Weissig, H., Westbrook, J. D., & Zardecki, C. (2002). The Protein Data Bank. *Acta crystallographica. Section D, Biological crystallography*, *58*(Pt 6 No 1), 899–907. https://doi.org/10.1107/s0907444902003451

26. Pertsemlidis, A., & Fondon, J. W., 3rd (2001). Having a BLAST with bioinformatics (and avoiding BLAST phemy). *Genome biology*, *2*(10), REVIEWS2002. https://doi.org/10.1186/gb-2001-2-10-reviews2002
27. Altschul, S. F., Gish, W., Miller, W., Myers, E. W., & Lipman, D. J. (1990). Basic local alignment search tool. *Journal of molecular biology*, *215*(3), 403–410. https://doi.org/10.1016/S0022-2836(05)80360-2
28. Altschul, S. F., Madden, T. L., Schäffer, A. A., Zhang, J., Zhang, Z., Miller, W., & Lipman, D. J. (1997). Gapped BLAST and PSI-BLAST: a new generation of protein database search programs. *Nucleic acids research*, *25*(17), 3389–3402. https://doi.org/10.1093/nar/25.17.3389
29. Przybylski, D., & Rost, B. (2008). Powerful fusion: PSI-BLAST and consensus sequences. *Bioinformatics (Oxford, England)*, *24*(18), 1987–1993. https://doi.org/10.1093/bioinformatics/btn384
30. Kerfeld, C. A., & Scott, K. M. (2011). Using BLAST to teach "E-value-tionary" concepts. *PLoS biology*, *9*(2), e1001014. https://doi.org/10.1371/journal.pbio.1001014
31. Cole, C., Barber, J. D., & Barton, G. J. (2008). The Jpred 3 secondary structure prediction server. *Nucleic acids research*, *36*(Web Server issue), W197–W201. https://doi.org/10.1093/nar/gkn238
32. Drozdetskiy, A., Cole, C., Procter, J., & Barton, G. J. (2015). JPred4: a protein secondary structure prediction server. *Nucleic acids research*, *43*(W1), W389–W394. https://doi.org/10.1093/nar/gkv332
33. Rost, B., Sander, C., & Schneider, R. (1994). Redefining the goals of protein secondary structure prediction. *Journal of molecular biology*, *235*(1), 13–26. https://doi.org/10.1016/s0022-2836(05)80007-5
34. Cuff, J. A., & Barton, G. J. (1999). Evaluation and improvement of multiple sequence methods for protein secondary structure prediction. *Proteins*, *34*(4), 508–519. https://doi.org/10.1002/(sici)1097-0134(19990301)34:4<508::aid-prot10>3.0.co;2-4
35. Söding, J., Biegert, A., & Lupas, A. N. (2005). The HHpred interactive server for protein homology detection and structure prediction. *Nucleic acids research*, *33*(Web Server issue), W244–W248. https://doi.org/10.1093/nar/gki408
36. Zimmermann, L., Stephens, A., Nam, S. Z., Rau, D., Kübler, J., Lozajic, M., Gabler, F., Söding, J., Lupas, A. N., & Alva, V. (2018). A Completely Reimplemented MPI Bioinformatics Toolkit with a New HHpred Server at its Core. *Journal of molecular biology*, *430*(15), 2237–2243. https://doi.org/10.1016/j.jmb.2017.12.007
37. Thompson, J. D., Gibson, T. J., Plewniak, F., Jeanmougin, F., & Higgins, D. G. (1997). The CLUSTAL_X windows interface: flexible strategies for multiple sequence alignment aided by quality analysis tools. *Nucleic acids research*, *25*(24), 4876–4882. https://doi.org/10.1093/nar/25.24.4876
38. Larkin, M. A., Blackshields, G., Brown, N. P., Chenna, R., McGettigan, P. A., McWilliam, H., Valentin, F., Wallace, I. M., Wilm, A., Lopez, R., Thompson, J. D., Gibson, T. J., & Higgins, D. G. (2007). Clustal W and Clustal X version 2.0. *Bioinformatics (Oxford, England)*, *23*(21), 2947–2948. https://doi.org/10.1093/bioinformatics/btm404
39. Sali, A., Potterton, L., Yuan, F., van Vlijmen, H., & Karplus, M. (1995). Evaluation

of comparative protein modeling by MODELLER. *Proteins*, *23*(3), 318–326. https://doi.org/10.1002/prot.340230306

40. Webb, B., & Sali, A. (2014). Comparative Protein Structure Modeling Using MODELLER. *Current protocols in bioinformatics*, *47*, 5.6.1–5.6.32. https://doi.org/10.1002/0471250953.bi0506s47
41. Kaplan, W., & Littlejohn, T. G. (2001). Swiss-PDB Viewer (Deep View). *Briefings in bioinformatics*, *2*(2), 195–197. https://doi.org/10.1093/bib/2.2.195
42. William L. Jorgensen, David S. Maxwell, & Julian Tirado-Rives. (**1996)** Development and Testing of the OPLS AllAtom Force Field on Conformational Energetics and Properties of Organic Liquids. *Journal of the American Chemical Society 118* (45), 11225-11236.
43. George A. Kaminski, Richard A. Friesner, Julian Tirado-Rives, and William L. Jorgensen. (2001). Evaluation and Reparametrization of the OPLSAA Force Field for Proteins via Comparison with Accurate Quantum Chemical Calculations on Peptides. *J. Phys. Chem.* B, 105, 6474-6487.
44. Feig M. (2016). Local Protein Structure Refinement via Molecular Dynamics Simulations with locPREFMD. *Journal of chemical information and modeling*, *56*(7), 1304–1312. https://doi.org/10.1021/acs.jcim.6b00222
45. DasGupta, D., Kaushik, R., & Jayaram, B. (2015). From Ramachandran Maps to Tertiary Structures of Proteins. *The journal of physical chemistry. B*, *119*(34), 11136–11145. https://doi.org/10.1021/acs.jpcb.5b02999
46. Zhou, A. Q., O'Hern, C. S., & Regan, L. (2011). Revisiting the Ramachandran plot from a new angle. *Protein science : a publication of the Protein Society*, *20*(7), 1166–1171. https://doi.org/10.1002/pro.644
47. Carrascoza, F., Zaric, S., & Silaghi-Dumitrescu, R. (2014). Computational study of protein secondary structure elements: Ramachandran plots revisited. *Journal of molecular graphics & modelling*, *50*, 125–133. https://doi.org/10.1016/j.jmgm.2014.04.001
48. Lakshmi, B., Ramakrishnan, C., Archunan, G., Sowdhamini, R., & Srinivasan, N. (2014). Investigations of Ramachandran disallowed conformations in protein domain families. *International journal of biological macromolecules*, *63*, 119–125. https://doi.org/10.1016/j.ijbiomac.2013.10.032
49. Kleywegt, G. J., & Jones, T. A. (1996). Phi/psi-chology: Ramachandran revisited. *Structure (London, Englan: 1993)*, *4*(12), 1395–1400. https://doi.org/10.1016/s0969-2126(96)00147-5
50. Eisenberg, D., Lüthy, R., & Bowie, J. U. (1997). VERIFY3D: assessment of protein models with three-dimensional profiles. *Methods in enzymology*, *277*, 396–404. https://doi.org/10.1016/s0076-6879(97)77022-8
51. Bowie, J. U., Lüthy, R., & Eisenberg, D. (1991). A method to identify protein sequences that fold into a known three-dimensional structure. *Science (New York, N.Y.)*, *253*(5016), 164–170. https://doi.org/10.1126/science.1853201
52. Lüthy, R., Bowie, J. U., & Eisenberg, D. (1992). Assessment of protein models with three-dimensional profiles. *Nature*, *356*(6364), 83–85. https://doi.org/10.1038/356083a0
53. Wiederstein, M., & Sippl, M. J. (2007). ProSA-web: interactive web service for the recognition of errors in three-dimensional structures of proteins. *Nucleic acids research*, *35*(Web Server issue), W407–W410. https://doi.org/10.1093/nar/gkm290
54. Laskowski, R. A., Hutchinson, E. G., Michie, A. D., Wallace, A. C., Jones, M. L., & Thornton, J. M. (1997). PDBsum: a Web-based database of summaries and

analyses of all PDB structures. *Trends in biochemical sciences*, *22*(12), 488–490. https://doi.org/10.1016/s0968-0004(97)01140-7

55. Binkowski, T. A., Naghibzadeh, S., & Liang, J. (2003). CASTp: Computed Atlas of Surface Topography of proteins. *Nucleic acids research*, *31*(13), 3352–3355. https://doi.org/10.1093/nar/gkg512
56. Dundas, J., Ouyang, Z., Tseng, J., Binkowski, A., Turpaz, Y., & Liang, J. (2006). CASTp: computed atlas of surface topography of proteins with structural and topographical mapping of functionally annotated residues. *Nucleic acids research*, *34*(Web Server issue), W116–W118. https://doi.org/10.1093/nar/gkl282
57. B-Rao, C., Subramanian, J., & Sharma, S. D. (2009). Managing protein flexibility in docking and its applications. *Drug discovery today*, *14*(7-8), 394–400. https://doi.org/10.1016/j.drudis.2009.01.003
58. Kontoyianni, M., McClellan, L. M., & Sokol, G. S. (2004). Evaluation of docking performance: comparative data on docking algorithms. *Journal of medicinal chemistry*, *47*(3), 558–565. https://doi.org/10.1021/jm0302997
59. Zahiri, J., Bozorgmehr, J. H., & Masoudi-Nejad, A. (2013). Computational Prediction of Protein-Protein Interaction Networks: Algo-rithms and Resources. *Current genomics*, *14*(6), 397–414. https://doi.org/10.2174/1389202911314060004
60. Rao, V. S., Srinivas, K., Sujini, G. N., & Kumar, G. N. (2014). Protein-protein interaction detection: methods and analysis. *International journal of proteomics*, *2014*, 147648. https://doi.org/10.1155/2014/147648
61. Schneidman-Duhovny, D., Inbar, Y., Nussinov, R., & Wolfson, H. J. (2005). PatchDock and SymmDock: servers for rigid and symmetric docking. *Nucleic acids research*, *33*(Web Server issue), W363–W367. https://doi.org/10.1093/nar/gki481
62. Villoutreix, B. O., Eudes, R., & Miteva, M. A. (2009). Structure-based virtual ligand screening: recent success stories. *Combinatorial chemistry & high throughput screening*, *12*(10), 1000–1016. https://doi.org/10.2174/138620709789824682
63. Waszkowycz B. (2008). Towards improving compound selection in structure-based virtual screening. *Drug discovery today*, *13*(5-6), 219–226. https://doi.org/10.1016/j.drudis.2007.12.002
64. Dallakyan, S., & Olson, A. J. (2015). Small-molecule library screening by docking with PyRx. *Methods in molecular biology (Clifton, N.J.)*, *1263*, 243–250. https://doi.org/10.1007/978-1-4939-2269-7_19
65. Aliabadi, A., Andisheh, S., Tayarani-Najaran, Z., & Tayarani-Najaran, M. (2013). 2-(4-Fluorophenyl)-N-phenylacetamide Derivatives as Anticancer Agents: Synthesis and In-vitro Cytotoxicity Evaluation. *Iranian journal of pharmaceutical research : IJPR*, *12*(3), 267–271.
66. Wang, Y., Suzek, T., Zhang, J., Wang, J., He, S., Cheng, T., Shoemaker, B. A., Gindulyte, A., & Bryant, S. H. (2014). PubChem BioAssay: 2014 update. *Nucleic acids research*, *42*(Database issue), D1075–D1082. https://doi.org/10.1093/nar/gkt978
67. Trott, O., & Olson, A. J. (2010). AutoDock Vina: improving the speed and accuracy of docking with a new scoring function, efficient optimization, and multithreading. *Journal of computational chemistry*, *31*(2), 455–461. https://doi.org/10.1002/jcc.21334
68. van de Waterbeemd, H., & Gifford, E. (2003). ADMET in silico modelling: towards prediction paradise?. *Nature reviews. Drug discovery*, *2*(3), 192–204. https://doi.org/10.1038/nrd1032
69. Moroy, G., Martiny, V. Y., Vayer, P., Villoutreix, B. O., & Miteva, M. A. (2012).

Toward in silico structure-based ADMET prediction in drug discovery. *Drug discovery today*, *17*(1-2), 44–55. https://doi.org/10.1016/j.drudis.2011.10.023

70. Di L. (2015). Strategic approaches to optimizing peptide ADME properties. *The AAPS journal*, *17*(1), 134–143. https://doi.org/10.1208/s12248-014-9687-3
71. Prueksaritanont, T., & Tang, C. (2012). ADME of biologics-what have we learned from small molecules?. *The AAPS journal*, *14*(3), 410–419. https://doi.org/10.1208/s12248-012-9353-6
72. Augustijns, P., Wuyts, B., Hens, B., Annaert, P., Butler, J., & Brouwers, J. (2014). A review of drug solubility in human intestinal fluids: implications for the prediction of oral absorption. *European journal of pharmaceutical sciences : official journal of the European Federation for Pharmaceutical Sciences*, *57*, 322–332. https://doi.org/10.1016/j.ejps.2013.08.027
73. Zhao, Y. H., Abraham, M. H., Le, J., Hersey, A., Luscombe, C. N., Beck, G., Sherborne, B., & Cooper, I. (2002). Rate-limited steps of human oral absorption and QSAR studies. *Pharmaceutical research*, *19*(10), 1446–1457. https://doi.org/10.1023/a:1020444330011
74. Lipinski, C. A., Lombardo, F., Dominy, B. W., & Feeney, P. J. (2001). Experimental and computational approaches to estimate solubility and permeability in drug discovery and development settings. *Advanced drug delivery reviews*, *46*(1-3), 3–26. https://doi.org/10.1016/s0169-409x(00)00129-0
75. Congreve, M., Carr, R., Murray, C., & Jhoti, H. (2003). A 'rule of three' for fragment-based lead discovery?. *Drug discovery today*, *8*(19), 876–877. https://doi.org/10.1016/s1359-6446(03)02831-9
76. Daina, A., Michielin, O., & Zoete, V. (2017). SwissADME: a free web tool to evaluate pharmacokinetics, drug-likeness and medicinal chemistry friendliness of small molecules. *Scientific reports*, *7*, 42717. https://doi.org/10.1038/srep42717
77. Daina, A., & Zoete, V. (2016). A BOILED-Egg To Predict Gastrointestinal Absorption and Brain Penetration of Small Molecules. *ChemMedChem*, *11*(11), 1117–1121. https://doi.org/10.1002/cmdc.201600182
78. Daina, A., Michielin, O., & Zoete, V. (2014). iLOGP: a simple, robust, and efficient description of n-octanol/water partition coefficient for drug design using the GB/SA approach. *Journal of chemical information and modeling*, *54*(12), 3284–3301. https://doi.org/10.1021/ci500467k
79. Jyothi Bandi., Navaneetha Nambigari. (2021). Identification of Novel Anticancer Agent by insilico Methods for Inhibition of KLK-12 Protein. *Asian J. Org. Med. Chem*., *6*(1), 13-23. https://doi.org/10.14233/ajomc.2021.ajomc-p304
80. Bandi, J., Malkhed, V. & Nambigari, N. (2022). An insilico study of KLK-14 protein and its inhibition with curcumin and its derivatives. *Chem. Pap. 76*, 4955–4966. https://doi.org/10.1007/s11696-022-02209-w
81. Lovering F, Bikker J, Humblet C (2009) Escape from Flatland: increasing saturation as an approach to improving clinical success*. J Med Chem.* https:// doi. org/ 10.

1021/ jm901 241e

82. Ritchie TJ, Ertl P, Lewis R (2011) The graphical representation of ADME-related molecule properties for medicinal chemists. *Drug Discov Today.* https:// doi. org/ 10. 1016/j. drudis. 2010. 11. 002

Supplementary Information

Table S1: Secondary structure data of KLK-15 protein.

Helices					
S. No.	Start Residue	End Residue	Helix type	No. of Residues	Residue sequence
1	Ala61	Cys63	G	3	AHC
2	Asp177	Ser183	H	7	DTSCDKS
3	Val242	Met253	H	12	VCHYLEWIRETM
Beta- sheets					
S. No.	Start Residue	End Residue	No. of Residues		Residue sequence
1	Lys21	Leu23	3		KLL
2	Asp26	Glu27	2		DE
3	Gln36	Glu41	6		QVALYE
4	Arg44	Leu51	8		RFNCGASL
5	Trp56	Ser59	4		WVLS
6	Arg69	Leu72	4		RVRL
7	Gln85	Pro94	10		QLRTTSRVIP
8	Met108	Leu112	5		MLLRL
9	Ala137	Gly142	6		ACVVSG
10	His168	Ile174	7		HCANISI
11	Met192	Gly196	5		MVCAG
12	GlU203	Cys205	3		ESC
13	Pro212	Cys215	4		PLVC
14	Ile218	Trp225	8		ILQGIVSW
15	Gly237	Lys241	5		GVYTK
Beta hairpins					
S. No.	Strand1			Strand 2		
	Start Residue	End Residue	No. of Residues	Start Residue	End Residue	No. of Residues
1	Gln36	Glu41	6	Arg44	Leu51	8
2	Arg44	Leu51	8	Trp56	Ser59	4
3	Arg69	Leu72	4	Gln85	Pro94	10
4	Gln85	Pro94	10	Met108	Leu112	5

5	Ala137	Gly142	6	His168	Ile174	7
6	His168	Ile174	7	Met192	Gly196	5
7	Pro212	Cys215	4	Ile218	Trp225	8
8	Ile218	Trp225	8	Met192	Lys241	5

Table S2. Structure of ligand molecules, Binding Energy and RMSD.

S. No.	Structure of Ligand with IUPAC name	E n e r g y (kcal/mol)	RMSD
L1	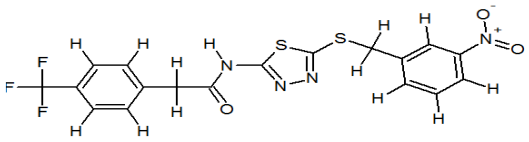 *N*-{5-[(3-nitrobenzyl)sulfanyl]-1,3-thiadiazol-2-yl}-2-[4-(trifluoromethyl)phenyl]acetamide	-7.6	0
L2	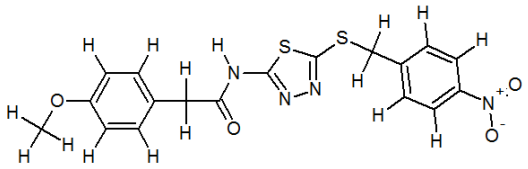 2-(4-methoxyphenyl)-*N*-{5-[(4-nitrobenzyl)sulfanyl]-1,3,4-thiadiazol-2-yl}acetamide	-7.1	0
L3	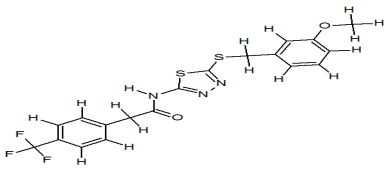 *N*-{5-[(3-methoxybenzyl)sulfanyl]-1,3,4-thiadiazol-2-yl}-2-[4-(trifluoromethyl)phenyl]acetamide	-7.1	0
L4	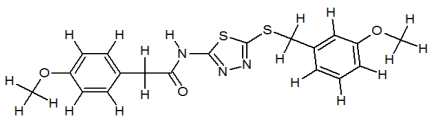 *N*-{5-[(3-methoxybenzyl)sulfanyl]-1,3,4-thiadiazol-2-yl}-2-(4-methoxyphenyl)acetamide	-6.8	1.412

L5	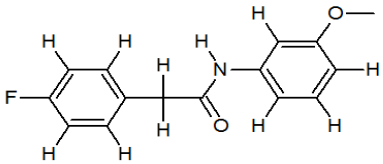 2-(4-fluorophenyl)-*N*-(3-methoxyphenyl)acetamide	-6.7	0
L6	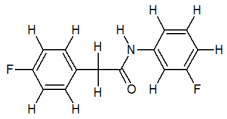 *N*-(3-fluorophenyl)-2-(4-fluorophenyl)acetamide *N*-(3-fluorophenyl)-2-(4-fluorophenyl)acetamide	-6.7	0
L7	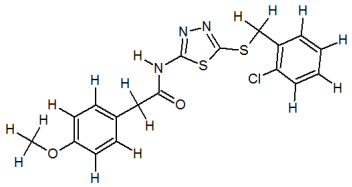 *N*-{5-[(2-chlorobenzyl)sulfanyl]-1,3,4-thiadiazol-2-yl}-2-(4-methoxyphenyl)acetamide *N*-{5-[(2-chlorobenzyl)sulfanyl]-1,3,4-thiadiazol-2-yl}-2-(4-methoxyphenyl)acetamide	-6.6	0
L8	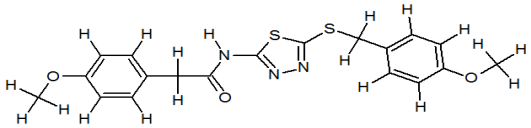 *N*-{5-[(4-methoxybenzyl)sulfanyl]-1,3,4-thiadiazol-2-yl}-2-(4-methoxyphenyl)acetamide *N*-{5-[(4-methoxybenzyl)sulfanyl]-1,3,4-thiadiazol-2-yl}-2-(4-methoxyphenyl)acetamide	-6.6	0
L9	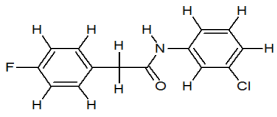 *N*-(3-chlorophenyl)-2-(4-fluorophenyl)acetamide *N*-(3-chlorophenyl)-2-(4-fluorophenyl)acetamide	-6.5	0

Current Trends in Biotechnology and Pharmacy
Vol. 20(2) 2913-2934 April 2026, ISSN 0973-8916 (Print), 2230-7303 (Online)
DOI: 10.5530/ctbp.2026.2.16